High-Speed Distance Relaying of the Entire Length of Transmission Lines without Signaling

Azizi, Sadegh; Sun, Mingyu; Liu, Gaoyuan; Popov, Marjan; Terzija, Vladimir

DOI
10.1109/TPWRD.2019.2957302

Publication date
2019

Document Version
Accepted author manuscript

Published in
IEEE Transactions on Power Delivery

Citation (APA)
Azizi, S., Sun, M., Liu, G., Popov, M., & Terzija, V. (2019). High-Speed Distance Relaying of the Entire Length of Transmission Lines without Signaling. *IEEE Transactions on Power Delivery*, *35 (2020)*(4), 1949-1959. Article 8920145. https://doi.org/10.1109/TPWRD.2019.2957302

This article has been accepted for publication in a future issue of this journal, but has not been fully edited. Content may change prior to final publication. Citation information: DOI 10.1109/TPWRD.2019.2957302, IEEE Transactions on Power Delivery

High-Speed Distance Relaying of the Entire Length of Transmission Lines without Signaling

Sadegh Azizi, *Senior Member, IEEE,* Mingyu Sun, *Student Member, IEEE,* Gaoyuan Liu, *Student Member, IEEE,* Marjan Popov, *Senior Member, IEEE,* and Vladimir Terzija, *Fellow, IEEE*

***Abstract*—Short-circuit faults close to either end of a transmission line, are normally cleared instantaneously by the distance relay at that end and after hundreds of milliseconds, *i.e.*, in Zone 2 operating time, by the relay at the opposite end of the line. This sequential tripping can be accelerated on condition that a reliable communication link is available for signaling between the two line ends. This paper proposes a novel non-communication method providing high-speed distance relaying over the entire length of the protected transmission line. The inputs to the method are the protected line parameters and local voltage and current signals measured by the relay, similar to those to conventional distance relays. The proposed method accomplishes Accelerated Sequential Tripping (AST) within a couple of cycles after the opening of the remote-end circuit breaker (ORCB) of the line. To achieve this, an accurate closed-form solution is derived for the fault distance in terms of post-ORCB voltage and current phasors. For the detection of the ORCB instant, a set of proper indices are proposed. This is to verify the fault distance calculated by the relay, before issuing a trip command. The proposed method is successfully validated by conducting more than 20000 hardware-in-the-loop (HIL) tests, and also using real-life data.**

***Index Terms*—Accelerated sequential tripping (AST), Distance relays, Opening of the remote-end circuit breaker (ORCB), Real-time digital simulator (RTDS).**

I. Introduction

THE reach of distance relays is not definite due to several sources of uncertainties such as inaccuracy of instrument transformers and the unknown value of fault resistance [1], [2]. Zone 1 of a distance relay is usually set in a way that it operates instantaneously for faults within the first 80%-90% of the protected line [3]. The line segment that remains unprotected by Zone 1 is called the *end-section*. To clear faults on the end-section, Zone 2 is introduced and is graded with an intentional time delay of *e.g.*, 400 ms to coordinate its operation with distance relays of neighboring lines [1]–[3].

Faults on the end-section of the protected line are cleared after a certain delay imposed by the Zone 2 settings. This results in non-simultaneous tripping of the circuit breakers (CBs) at the opposite line ends, which is known as *sequential tripping* [2]. Considering the CB operating time, the fault remains supplied under sequential tripping from one end of the line for more than the Zone 2 operating time. This would cause delayed auto-reclosing and might even endanger system stability [1], [2]. That is why signaling is used, if possible, to send a transfer trip signal to the remote-end relay for having the remote-end CB open as quickly as possible [1], [4]. Accordingly, faults on the end-section are cleared faster than in the Zone 2 operating time. Due to communication delays, AST is slower than the ideal simultaneous instantaneous tripping (SIT) of the CBs at the opposite line ends, but still falls under high-speed fault clearing [5].

Non-communication AST schemes have the advantage of not relying upon costly communication infrastructure needed for signaling. This is why various non-communication AST schemes have been proposed, thus far [6]–[20]. These methods can be classified into two major groups, depending on whether their functionality is based on the fundamental phasors, or fault generated high-frequency transient components of voltage and current signals. Methods based on transient components require a very high sampling frequency, which increases the cost of their deployment [6]–[8]. Fundamental-phasor based methods are considered more practical, as they use voltage and current fed to traditional distance relays [9]–[20].

The AST technique presented in [9] uses the mutual coupling characteristics between faulted and sound phases. Reference [11] takes advantage of the fact that in heavy loading condition, ORCB can change the X/R ratio as well as active and reactive powers measured by the relay. The methods presented in [12], [13] provide AST for end-section faults by interpreting the variations of negative- and zero-sequence currents following ORCB. A series of logics attributed to the balanced/imbalanced operation of the system is used in [16], [17] in order to detect ORCB. The methods proposed in [18], [20] are based on the direction of impedance change seen by the phase and ground elements of the distance relay.

The derivations of existing fundamental-phasor based algorithms rely on one or more of the following assumptions:

- Abrupt changes in the post-fault voltage and current signals originate from the opening of line CBs only.
- Specific line loading condition holds before the fault

S. Azizi is with the School of Electronic and Electrical Engineering, University of Leeds, Leeds, England, UK (e-mail: s.azizi@leeds.ac.uk).

M. Sun, G. Liu, and V. Terzija are with the School of Electrical and Electronic Engineering, University of Manchester, Manchester, England, UK (e-mail: mingyu.sun@manchester.ac.uk; gaoyuan.liu@manchester.ac.uk; vladimir.terzija@manchester.ac.uk).

M. Popov is with the Faculty of Electrical Engineering, Mathematics and Computer Science, Delft University of Technology, Delft, Netherlands (e-mail: m.popov@tudelft.nl).

This article has been accepted for publication in a future issue of this journal, but has not been fully edited. Content may change prior to final publication. Citation information: DOI 10.1109/TPWRD.2019.2957302, IEEE Transactions on Power Delivery

inception.

- The ratio between the zero- and positive-sequence impedances of the rest of the network is equal to, greater than or less than a certain value.
- The mutual coupling between the sound and faulty phases of the faulted line can be neglected.
- Fault resistance lies within a specific narrow range.
- Mode of the CB opening, *i.e.*, three-pole or single-pole, is known to the relay.

The above-mentioned phasor-based methods are effective so long as their overlaying assumptions hold. However, the first four assumptions outlined might or might not apply depending on operating condition, system parameters and the chain of events the power system may undergo. Fault resistance is a random variable and can take any value within a wide range. To improve stability, the single-pole opening of CBs may be enabled for single-phase-to-ground (1-ph-g) faults. Nonetheless, this does not guarantee that CBs will always open single-pole under 1-ph-g faults since the relay might identify the fault type incorrectly.

This paper is focused on 1-ph-g faults, as the most frequent fault type in transmission systems. For this type of faults on the line end-section, sequential tripping of the faulted line is accelerated by resetting for them the intentional time delay of Zone 2 to 0 sec. To detect the ORCB instant, two sets of proper indices are proposed. A trip command is issued once ORCB is detected and the estimated fault distance lies within the protected line length. The proposed method is not sensitive to pre-fault line loading, system parameters or the magnitude of fault resistance. This method can easily be extended to other fault types and performs desirably, irrespective of whether ORCB is single- or three-pole.

II. Distance Relays and Sequential Tripping

Fig. 1(a) shows the single-line diagram of a two-source system under normal condition. The surrounding active network is modeled by its Thevenin equivalent. Figs 1(b) and 1(c) represent the single-line diagram of the same system during a fault at distance α from the sending-end terminal of the line, before and after ORCB, respectively. The time periods associated to the circuits of Figs 1(a), 1(b) and 1(c) are referred to as the pre-fault, pre-ORCB and post-ORCB fault periods, respectively. The superscripts pre, $fault$ and $post$ of voltage and current phasors refer to these signals in the pre-fault, pre-ORCB fault and post-ORCB circuits, respectively. The subscripts s, r and f are used to denote the terminal or spot on the line to which a variable is attributed.

A. Modeling ORCB under Single-Phase-to-Ground Faults

While the fault type determines how the sequence circuits are to be interconnected, each sequence circuit can also be

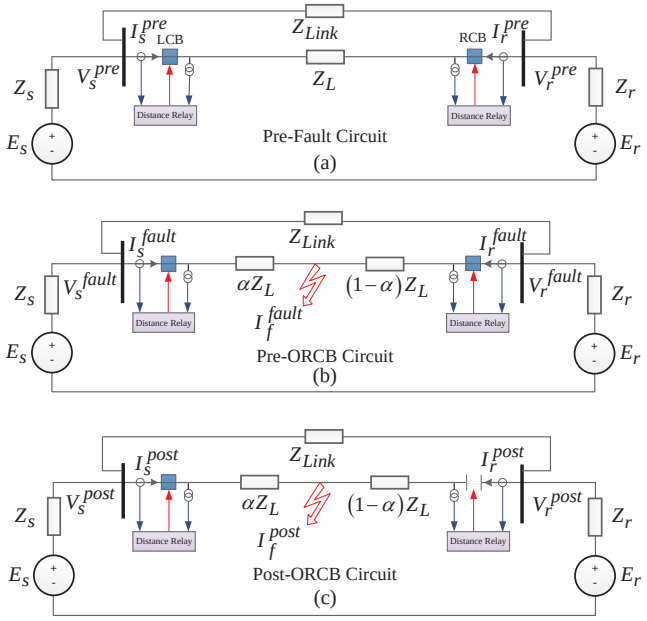

Fig. 1. Single-line diagram of a two-source system (a) Under normal condition, (b) During a fault and before the opening of the remote-end circuit breaker (ORCB), (c) During a fault and after ORCB.

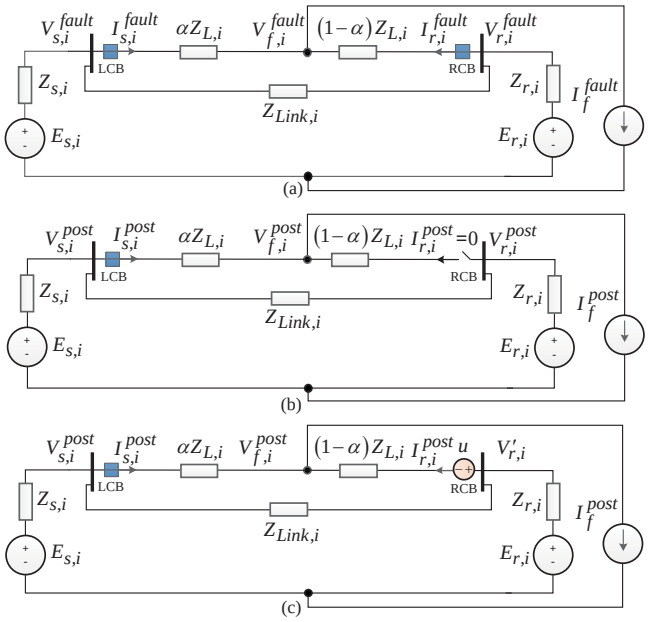

Fig. 2. Individual analysis of the sequence circuit i under a 1-ph-g short-circuit fault on the line s-r (a) Before ORCB, (b) During fault and after three-pole ORCB, (c) During fault and after single-pole ORCB.

studied individually thanks to the substitution theorem of *Circuit Theory* [21]. Fig. 2 shows the circuits used in this paper for the individual analysis of each sequence circuit under a 1-ph-g fault; for (a) before ORCB, (b) after three-pole ORCB, and (c) after single-pole ORCB. The subscript i takes a value of 0, 1 or 2 and refers to the zero-, positive- and negative-sequence circuits, respectively. Besides, $Z_{L,i}$ is the series impedance of the protected line in the sequence circuit i. The value of $E_{s,i}$ and $E_{r,i}$ are set to zero for $i = 0$ and $i = 2$ as the zero- and negative-sequence circuits contain no

This article has been accepted for publication in a future issue of this journal, but has not been fully edited. Content may change prior to final publication. Citation information: DOI 10.1109/TPWRD.2019.2957302, IEEE Transactions on Power Delivery

active sources. The current source in each circuit of Fig. 2 has essentially been substituted for the series connection of the fault resistance and two other sequence circuits.

To detail the *A-g* element of the proposed distance relay, phase *A* is taken as the reference in all equations presented below. For equations of the *B-g* and *C-g* elements of the relay, phase *B* and phase *C* should be taken as the reference, respectively. Three-pole ORCB is modeled by opening the remote end of the line in all sequence circuits, as shown in Fig. 2(b). Single-pole ORCB is modeled in this paper by replacing the RCB by an unknown voltage source, which is identical in all sequence circuits. To justify this, let the superscripts A, B, C and 0, 1, 2 denote variables of the respective phase and sequence circuits. Subsequent to single-pole ORCB, the current of the opened phase drops to zero, and the zero voltage across the RCB contacts of the two non-faulted phases remains unchanged. This means that following a 1-ph-g fault on phase A, the relationships below hold:

$$\begin{cases} u_B^{post} = u_C^{post} = 0 \\ I_{r,A}^{post} = 0 \end{cases} \tag{1}$$

Using the method of symmetrical components, the following relationships can be obtained from (1):

$$\begin{cases} u_0^{post} = u_1^{post} = u_2^{post} \\ I_{r,0}^{post} + I_{r,1}^{post} + I_{r,2}^{post} = 0 \end{cases} \tag{2}$$

According to the first equation of (2), the RCB in all sequence circuits may be replaced by a similar voltage source u, as shown in the circuit of Fig. 2(c). The node voltages and branch currents in this circuit can be expressed as functions of the unknown variable u. The value of u can be readily obtained using the second equation of (2). This yields the currents and voltages of the post-ORCB circuit.

B. Accurate Fault Location Following ORCB

In this subsection, the relation between voltage and current phasors measured by the relay and the fault distance is derived. The obtained closed-form solution for the fault distance applies under both single- and three-pole ORCB.

After three-pole ORCB, the receiving-end currents of the protected line become zero. Therefore, the three-pole ORCB is modeled by opening that end of the line in all sequence circuits. By applying KCL at the fault location in all sequence circuits before and after the three-pole ORCB, one obtains:

$$\begin{cases} I_f^{fault} = I_{s,i}^{fault} + I_{r,i}^{fault} \\ I_f^{post} = I_{s,i}^{post} \end{cases} \quad \forall i = 0, 1 \text{ or } 2 \tag{3}$$

Single-pole tripping of faulted lines is an effective practice improving system stability following 1-ph-g faults in transmission systems [3]. From Fig. 2(c) and the second equation of (2), one can write [22]

$$I_f^{post} = \frac{I_{s,0}^{post} + I_{s,1}^{post} + I_{s,2}^{post}}{3} \tag{4}$$

It can be easily confirmed that (4) holds for the three-pole ORCB, also. The relationship between voltage at the fault location and sending-end voltage in the sequence circuit i is:

$$V_{f,i}^{post} = V_{s,i}^{post} - \alpha Z_{L,i} I_{s,i}^{post} \tag{5}$$

Denoting the fault resistance by R_f and taking (4) into account, one obtains

$$V_{f,0}^{post} + V_{f,1}^{post} + V_{f,2}^{post} = (I_{s,0}^{post} + I_{s,1}^{post} + I_{s,2}^{post}) R_f \tag{6}$$

By adding (5) written for all three sequence circuits, we have

$$\overbrace{(Z_{L,0} I_{s,0}^{post} + Z_{L,1} I_{s,1}^{post} + Z_{L,2} I_{s,2}^{post})}^{U_{s,A}^{post}} \alpha + \underbrace{(I_{s,0}^{post} + I_{s,1}^{post} + I_{s,2}^{post})}_{I_{s,A}^{post}} R_f = \underbrace{V_{s,0}^{post} + V_{s,1}^{post} + V_{s,2}^{post}}_{V_{s,A}^{post}} \tag{7}$$

Equation (7) relates the fault distance and resistance to the sending-end voltage and current phasors of the faulted line.

C. Closed-Form Solutions for Fault Distance and Resistance

Let us rewrite (7) in the following compact form:

$$U_{s,A}^{post} \alpha + I_{s,A}^{post} R_f = V_{s,A}^{post} \tag{8}$$

where $U_{s,A}^{post}$, $I_{s,A}^{post}$ and $V_{s,A}^{post}$ are complex variables, which are known through measurements, and α and R_f are real unknown variables. By separating the real and imaginary parts of (8), two new real equations can be obtained in terms of α and R_f. Solving this system of equations gives the following closed-form solutions for the fault distance and resistance:

$$\begin{bmatrix} \alpha \\ R_f \end{bmatrix} = \begin{bmatrix} \mathrm{Re}(U_{s,A}^{post}) & \mathrm{Re}(I_{s,A}^{post}) \\ \mathrm{Im}(U_{s,A}^{post}) & \mathrm{Im}(I_{s,A}^{post}) \end{bmatrix}^{-1} \begin{bmatrix} \mathrm{Re}(V_{s,A}^{post}) \\ \mathrm{Im}(V_{s,A}^{post}) \end{bmatrix} \tag{9}$$

It should be noted that (8) is formed based upon voltage and current signals taken after ORCB, hence the superscript $post$. This means a prerequisite to being able to use the closed-form solution (9) is knowing the ORCB instant.

III. Proposed Distance Relaying

In this section, firstly, the logic block diagram of the proposed distance relay is presented. Then, differences between the ideal phasors appearing in the equations of the previous section and those obtained from voltage and current waveforms measured by the relay are discussed. Finally, indices developed for detecting the ORCB instant and confirming the validity of the obtained fault distance, are presented.

This article has been accepted for publication in a future issue of this journal, but has not been fully edited. Content may change prior to final publication. Citation information: DOI 10.1109/TPWRD.2019.2957302, IEEE Transactions on Power Delivery

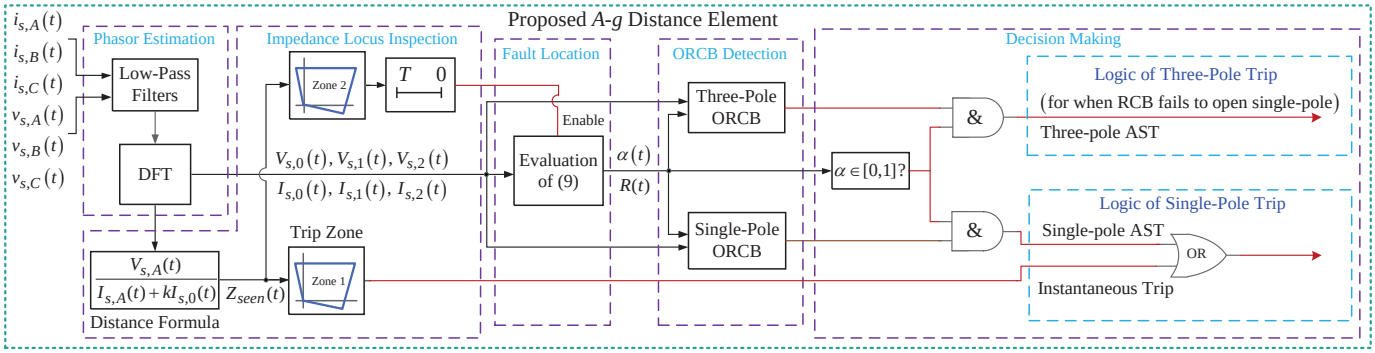

Fig. 3. Logic diagram of the A-g element of the proposed high-speed distance relay.

A. Logic Block Diagram of the Proposed Distance Relay

Fig. 3 shows the logic block diagram of the A-g element of the proposed high-speed distance relay. The block diagrams of the B-g and C-g elements have similar structures. The phase element of the proposed relay is identical to that of conventional distance relays. It is firstly assumed that single-pole tripping of transmission lines is intended in the case of 1-ph-g faults. Next, the modification needed for when single-pole tripping is not allowed is addressed.

The proposed distance relay consists of five separate components, as shown in Fig. 3. The phasor estimation and inspection of the impedance locus components replicate those of conventional distance relays. For Zone 1 faults, the trip command is issued instantaneously. The relay is intended to distinguish end-section Zone 2 faults from external Zone 2 faults. The fault location process is activated for Zone 2 faults once a certain time has elapsed since the fault inception. This is to account for the transition period of phasor estimation, thereby avoiding incorrect decision-making based on the erroneous fault distance calculated within this period.

The estimated distance by (9) is not considered valid before the detection of ORCB. On the other hand, the detection of ORCB alone is not conclusive enough to open the LCB based only upon. One main reason for this is the possibility of incorrect detection of ORCB. Another reason is the likelihood of maloperation of the remote-end relay to which the local relay must not respond. Therefore, the fault distance should be checked to be on the protected line, before generating a trip command to LCB. This is to prevent the relay from incorrect operation under external faults.

In case single-pole ORCB is not allowed, the logic block diagram of the distance relay should be slightly modified. To this end, the logic of single-pole trip of the block diagram presented in Fig. 3 is removed. Besides, the three-pole AST command is merged with the instantaneous trip command using an AND gate. In this way, faults in Zone 1 would be cleared three-pole instantaneously from both line-ends; the three-pole AST is provided for faults seen in Zone 1 from one line-end, and in Zone 2 from the opposite line-end.

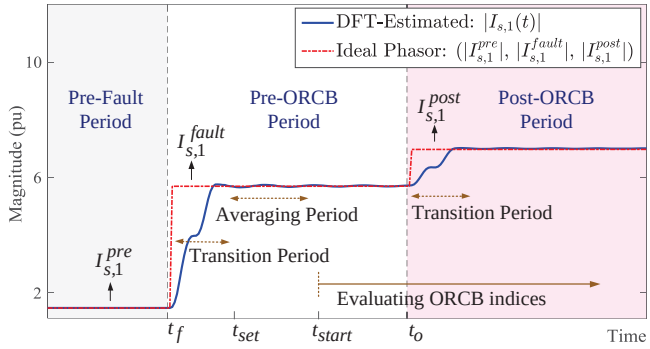

Fig. 4. Magnitudes of true and estimated positive-sequence phasors of sending-end current of line 9-8 for a fault at 70% of the line length.

B. Phasor Estimation and Related Technical Considerations

The sequence circuits studied in the previous section are assumed to be linear time-invariant circuits with sinusoidal inputs of the same frequency. This means the voltage and current response of these circuits, *i.e.*, the phasors marked with the superscripts pre, $fault$ and $post$, can be obtained most efficiently by the Phasor Method [21]. In practice, however, there is no distinct sequence circuit for different time periods, and we are dealing with one three-phase power system undergoing the fault and then ORCB. Besides, the parameters of the three-phase system of interest, except for the protected line parameters, are not normally available to the relay.

Let t_f and t_o be the fault inception and ORCB instants, respectively. Not knowing these instants, the relay continuously measures three-phase sending-end voltage and current waveforms and estimates their fundamental-frequency phasors over time. Estimated phasors are ideally expected to match their corresponding true phasors during the respective periods. For instance, if $I_{s,i}(t)$ is the sending-end current of the faulted line estimated at the instant t, it is desirable to have:

$$I_{s,i}(t) = \begin{cases} I_{s,i}^{pre} & \forall\ t < t_f \\ I_{s,i}^{fault} & \forall t_f \le t < t_o \\ I_{s,i}^{post} & \forall t_o \le t \end{cases} \quad \forall i = 0, 1 \text{ or } 2 \qquad (10)$$

In this paper, the discrete Fourier transform (DFT) is used to estimate fundamental-frequency phasors of time-domain

This article has been accepted for publication in a future issue of this journal, but has not been fully edited. Content may change prior to final publication. Citation information: DOI 10.1109/TPWRD.2019.2957302, IEEE Transactions on Power Delivery

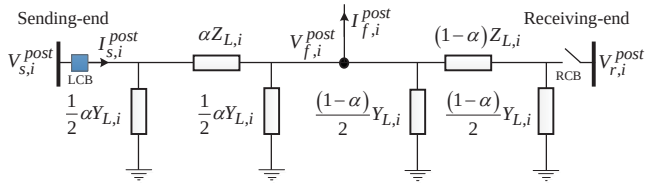

Fig. 5. Nominal π model of the two sections of the faulted line in the sequence circuit i, after three-pole ORCB.

waveforms. Similar to other phasor estimation methods, DFT is essentially a non-ideal filter. Upon any abrupt change in the magnitude and/or phase angle of an input waveform, its DFT-estimated phasor takes some time to settle at its new steady-state value. This time, being equal to the DFT window length, is referred to as transition period. Fig. 4 shows, as an example, the magnitudes of true and DFT-estimated positive-sequence current phasors associated to a fault on line 9-8 in the 39-bus test system [23]. The true and DFT-estimated phasors are shown in dash-dotted red and blue, respectively. As can be seen, the DFT-estimated phasor (blue curve) moves toward its new steady-state value (dash-dotted line) subsequent to the fault inception and ORCB. Once the transition period passes, the estimated phasor settles to its corresponding true value.

Phasors estimated within the first couple of cycles after the fault inception are generally less accurate than those estimated afterwards when the decaying dc and fault-generated harmonics of waveforms are damped out [1]. Averaging the estimated phasor over a time period is an effective way to alleviate its undesirable transient oscillations. This technique is employed here to more reliably represent pre-ORCB voltage and current phasors, *i.e.*, those with the $fault$ superscript. The time argument of estimated phasors is dropped when they are averaged over the averaging period, *e.g.*, from t_{set} to t_{start}. Not to mistake the averaged phasors with their corresponding true phasors, a bar sign is used with the former.

C. ORCB Detection

The system of equations (8) can be formed at any time instant but would be valid only if built based upon post-ORCB phasors. Hence, (9) gives the true fault distance once the RCB has opened. On the other hand, the RCB may open at any instant within the next couple of cycles after t_{start}. Two sets of indices are proposed here for detection of three- and single-pole ORCB, thereby confirming the fault distance obtained.

1) Three-Pole ORCB : After three-pole ORCB, the fault will be supplied only from the sending-end of the line in all sequence circuits. Under a 1-ph-g fault, the positive, negative- and zero-sequence fault currents are equal, which means:

$$I_{f,0}^{post} = I_{f,1}^{post} = I_{f,2}^{post} \tag{11}$$

With reference to the circuit in Fig. 5, one can obtain

$$I_{f,i}^{post} = (I_{s,i}^{post} - \frac{1}{2}\alpha Y_{L,i} V_{s,i}^{post}) - Y_{End,i}\left(V_{s,i}^{post} - \alpha Z_{L,i}(I_{s,i}^{post} - \frac{1}{2}\alpha Y_{L,i} V_{s,i}^{post})\right) \tag{12}$$

where $Y_{L,i}$ is the shunt admittance of the protected line in the sequence circuit i, and

$$Y_{End,i} = \frac{1}{2}Y_{L,i} + \left((1-\alpha)Z_{L,i} + \frac{2}{(1-\alpha)Y_{L,i}}\right)^{-1} \tag{13}$$

As the three fault currents in (11) are identical, the sum of their differences will be zero. Conversely, if these phasors were not identical, the sum of the absolute value of their differences would be non-zero. Accordingly, the closeness of the fault currents in the three sequence circuits can be used for detecting three-pole ORCB. To do so, the following normalized index is defined on the phasors estimated over time:

$$K_{3P}(t) = \frac{\sum_{i=0}^{2}\sum_{j>i}^{2}|I_{f,i}(t) - I_{f,j}(t)|}{\sum_{i=0}^{2}|I_{f,i}(t)|} \tag{14}$$

Before ORCB, the fault currents obtained based only on the sending-end currents without knowing the receiving-end ones, and the incorrect α and R_f calculated, will be different from the true fault current. Hence, the so-calculated currents will not be equal, as opposed to the true fault currents in different sequence circuits. Therefore, the three-pole ORCB can be confirmed only after (14) drops to zero.

2) Single-Pole ORCB : After single-pole ORCB, the magnitude and phase-angle of sending- and receiving-end voltage and current phasors may increase or decrease depending on different factors. Thus, no simple rule can be derived based on such changes in order to reliably infer the single-pole ORCB with. To propose reliable single-pole ORCB indices, a deeper analysis of the single-pole ORCB is needed. To this end, let us assume the variable ΔI denotes the change of the fault current after single-pole ORCB. Hence, the fault currents before and after single-pole ORCB will have the following relationship

$$I_f^{post} = I_f^{fault} + \Delta I \tag{15}$$

Let us assume that the fault current is divided between the sending-end and receiving-end of the faulted line in proportion to β_i and $(1-\beta_i)$. For before ORCB, one can write

$$\begin{cases} I_{s,i}^{fault} = \beta_i I_f^{fault} \\ I_{r,i}^{fault} = (1-\beta_i) I_f^{fault} \end{cases} \tag{16}$$

Assume that $Z_{Loop.i}$ denotes the impedance of the loop through which the post-ORCB current produced by u circulates. This loop is the path created by open-circuiting the voltage sources in the circuit of Fig. 2(c). According to the superposition theorem [21], the post-ORCB sending- and

This article has been accepted for publication in a future issue of this journal, but has not been fully edited. Content may change prior to final publication. Citation information: DOI 10.1109/TPWRD.2019.2957302, IEEE Transactions on Power Delivery

receiving-end currents of the faulted line in the sequence circuit i can be obtained from:

$$\begin{cases} I_{s,i}^{post} = \beta_i I_f^{post} + \frac{u}{Z_{Loop,i}} \\ I_{r,i}^{post} = (1-\beta_i) I_f^{post} - \frac{u}{Z_{Loop,i}} \end{cases} \tag{17}$$

where u is the voltage source representing the single-pole ORCB, as explained in section II.

With reference to Fig. 2(a) and the fault type being 1-ph-g, the receiving-end current of the faulted line before ORCB can be calculated from:

$$\alpha U_{s,A}^{fault} + 3R_f(I_{s,i}^{fault} + I_{r,i}^{fault}) = V_{s,A}^{fault} \tag{18}$$

On the other hand, it can be concluded from (4) and Fig. 2(c) that after single-pole ORCB,

$$I_{r,i}^{post} = \frac{1}{3}\sum_{j=0}^{2} I_{s,j}^{post} - I_{s,i}^{post} \tag{19}$$

The major problem with the foregoing two formulas is that the superscripts $fault$ and $post$ are applicable only if the ORCB instant is known. In practice, such discrimination cannot be applied to the phasors continuously estimated by the relay over time, *i.e.*, $I_{s,i}(t)$ and $V_{s,i}(t)$. To overcome this issue, let us define the two expressions below using the phasors and parameters estimated over time:

$$F_i(t) = \frac{\overbrace{\sum_{j=0}^{2} \bar{V}_{s,j}^{fault}}^{\bar{V}_{s,A}^{fault}} - \alpha(t) \overbrace{\sum_{j=0}^{2} Z_{L,j} \bar{I}_{s,j}^{fault}}^{\bar{U}_{s,A}^{fault}}}{3R(t)} - \bar{I}_{s,i}^{fault} \tag{20}$$

$$D_i(t) = \frac{1}{3}\sum_{j=0}^{2} I_{s,j}(t) - I_{s,i}(t) \tag{21}$$

where the bar sign refers to the average of corresponding phasors estimated over the period from t_{set} to t_{start}. The fault distance and resistance are estimated from (9) at each time instant, using the DFT-estimated phasors at that time instant. Thus, the estimates of α and R_f are functions of time and might be slightly oscillatory within the first couple of cycles after the fault inception. This is why they are used with a time argument in (20) and (21).

As will be demonstrated in Appendix A, we have

$$\begin{cases} F_i(t) = D_i(t) = \gamma_i I_f^{fault}, & \forall t_f \le t < t_o \\ F_i(t) = I_{r,i}^{fault}, & \forall t_o \le t \\ D_i(t) = I_{r,i}^{post}, & \forall t_o \le t \end{cases} \tag{22}$$

where

$$\gamma_i = \frac{1}{3}\sum_{j=0}^{2} \beta_j - \beta_i, \quad \forall i = 0, 1 \text{ or } 2 \tag{23}$$

For $t \ge t_o$, (20) and (21) yield the estimates of $I_{r,i}^{fault}$ and $I_{r,i}^{post}$, respectively. On the other hand, the magnitude of β_i takes small values for faults close to the receiving-end of the faulted line. This means γ_i would be small, ideally zero, under such faults. Subsequent to single-pole ORCB, the magnitude of (21) rises up from a small value to the magnitude of the post-fault receiving-end current. Simulation results show that, in general, this change of magnitude is more prevalent in the zero-sequence circuit than in the negative-sequence circuit. This is because the magnitude of the impedance of the zero-sequence loop is generally much larger than that of the negative-sequence loop. For simplicity, only $|D_0(t)|$ is used here as an indicator of single-pole ORCB.

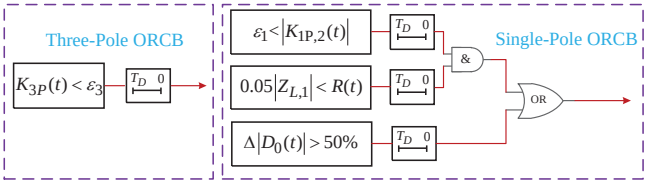

Fig. 6. Logic diagram of the three- and single-pole ORCB detection blocks.

The impedances of branches of the fault circuit are mainly inductive in practice. It follows that the term $\frac{u}{Z_{Loop,i}}$ involved in the post-ORCB currents in (17) is nearly in phase with the sending-end current and in opposite-phase with the receiving-end current. According to (22), (20) and (21) give rise to the same complex value for $t < t_o$. Taking advantage of these two properties, the following expression is introduced as another index for the detection of single-pole ORCB:

$$K_{1P,i}(t) = \left| \frac{I_{s,i}(t)}{D_i(t)} \right| - \left| \frac{\bar{I}_{s,i}^{fault}}{F_i(t)} \right| \tag{24}$$

Before ORCB, the two terms on the right-hand side of (24) are identical, and hence, their subtraction would be zero. After single-pole ORCB, the first and second terms on the right-hand side of (24) will not be equal anymore, which makes $K_{1P,i}$ non-zero. Accordingly, a magnitude change of greater than a prespecified value in $K_{1P,i}$ is considered an indicator of single-pole ORCB.

Following three- and single-pole ORCB, the indices K_{3P} and $K_{1P,i}$ will respectively drop to and rise from zero, initiating a trip command. The thresholds ϵ_3 and ϵ_1 are used to detect the variation of the proposed indices, and can be set to any positive small values. In practice, these thresholds should be set in a way as to account for a couple of percent of error that may be possibly introduced into estimated phasors.

3) Logic Diagram of ORCB Detection: Fig. 6 shows the logic diagram of ORCB detection using the indices proposed. To confirm three-pole ORCB, the index K_{3P} should fall below the prespecified small value ϵ_3 for a period of T_D, which is set to 10 ms here. Single-pole ORCB is confirmed once $|D_0(t)|$ faces 50% increase with respect to its primary value at the initial couple of cycles after the fault inception. In addition to this, $K_{1P,2}$ exceeding a predetermined small value is taken as an indicator of single-pole ORCB. The negative-sequence

This article has been accepted for publication in a future issue of this journal, but has not been fully edited. Content may change prior to final publication. Citation information: DOI 10.1109/TPWRD.2019.2957302, IEEE Transactions on Power Delivery

index is utilized for this sake since simulation results show its change is larger than that of the zero-sequence index. The time delay for certifying single-pole ORCB is considered to be T_D, as in certifying three-pole ORCB.

For faults with a zero resistance, the calculated fault distance using (9) would be accurate both before and after ORCB. To take advantage of this property, if the estimated fault resistance remains negligible for a long time, *e.g.*, 100 ms, the trip command is issued. This is to have the relay trip the LCB for internal faults, even in rare cases in which the relay would delay the detection of or possibly fail to detect ORCB. It should be noted that coordinating the proposed relay with the reclosing scheme is not a matter of concern, as it can be done in a similar way as that for conventional distance relays.

If the remote-end relay maloperates and unnecessarily opens the RCB for an external fault or when there has been no fault, the LCB must not open [2]. This is automatically guaranteed in conventional distance relaying with or without communication, because after an incorrect ORCB, the impedance seen by the local relay immediately moves out of its trip-zone [3]. In the proposed method, this is ensured by checking if the estimated fault distance lies within the protected line range. If not, it means the RCB has opened incorrectly and no trip command should be generated by the local relay.

IV. Performance Evaluation

In this section, the performance of the proposed distance relay is evaluated. In the first two subsections, real time digital simulator (RTDS) is used to conduct an extensive number of simulations and hardware-in-the-loop (HIL) testing. To do so, a generic 230 kV two-source system, as well as the New England 39-bus system [23] are used as test systems. In the last part, the voltage and current waveforms recorded during a real 1-ph-g fault incident are fed to the proposed relay to demonstrate its superiority over conventional distance relays.

The test systems are modeled using RSCAD and then loaded on a rack of RTDS, which includes five dual-core PB5 processor cards. Furthermore, two distance relays are modeled using RSCAD and loaded on another RTDS rack. The test system and relay racks are physically wired to each other to provide the relays with voltage and current waveforms of interest, and to connect the relays to the associated CBs in the test systems. Generated waveforms are passed through a second-order Butterworth anti-aliasing filter with a cut-off frequency of 400 Hz. The filtered signals are sampled with a sampling rate of 3200 Hz. The DFT along with a digital mimic filter for the removal of the decaying DC component from current signals [24] is used to estimate the fundamental-frequency phasors of voltage and current waveforms.

The portion of the line length for which fast fault clearing is provided, through simultaneous instantaneous tripping (SIT) or AST, is defined as the high-speed coverage of the relaying

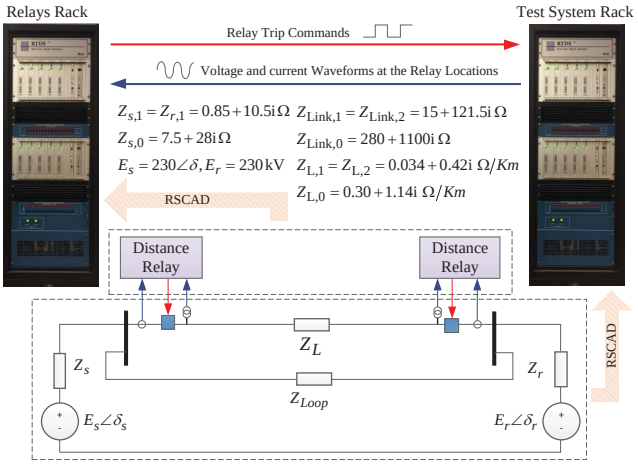

Fig. 7. Two-source RTDS test setup for HIL testing of the proposed relay.

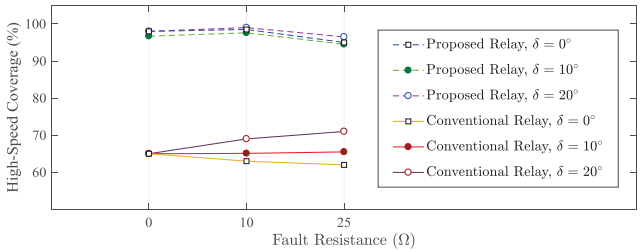

Fig. 8. High-speed coverage of the protected line by conventional and proposed distance relays under different transmission angels and fault resistances.

scheme. The intentional time delay of Zone 2 is set to 300 ms. Protection of the system by conventional and proposed distance relays are compared with each other in terms of high-speed coverage and average fault clearing time they offer.

A. Testing of the Robustness of the Proposed Distance Relay

The generic two-source test setup shown in Fig. 7 is used for performance evaluation of the proposed method. A large number of 1-ph-g faults are applied at 50 different locations on the protected 100-km long line. The arc is modeled by the empirical formula of [25] and put in series with fixed fault resistances of different value. For the power angle, *i.e.*, $\delta_s - \delta_r$, three values of 0°, 10° and 20° are tested. Each of the two source impedances is set to be 50%, 100% or 200% of their base values shown in Fig. 7. The averaging period starts 20 ms after the fault inception and ends 10 ms later. Fig. 8 compares the high-speed coverage of the proposed and conventional distance relays for different power angles and fault resistances.

Here, a 1-ph-g fault with a resistance of 25 Ω at 85% of the line length is considered as an example. The fault distance and resistance estimated before and after single-pole ORCB are shown in Fig. 9. As can be seen, the estimated fault distance converges to its true value following ORCB. Fig. 10 shows how the three-pole ORCB index drops to zero following ORCB. The opposite is true for the single-pole ORCB index, as it rises from zero following single-pole ORCB. Extensive

This article has been accepted for publication in a future issue of this journal, but has not been fully edited. Content may change prior to final publication. Citation information: DOI 10.1109/TPWRD.2019.2957302, IEEE Transactions on Power Delivery

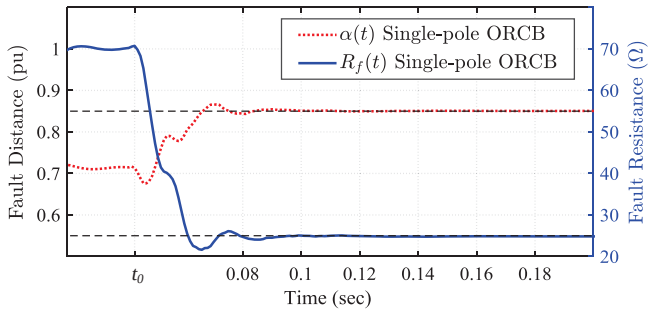

Fig. 9. Estimated fault distance and resistance following a 1-ph-g fault.

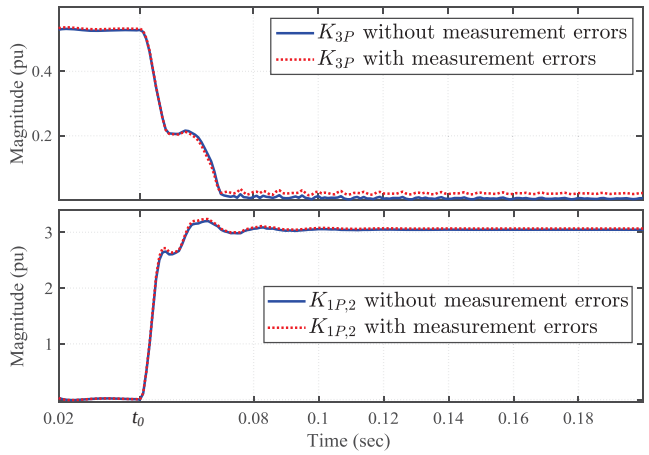

Fig. 10. Evaluation of the ORCB indices following single- and three-pole ORCB.

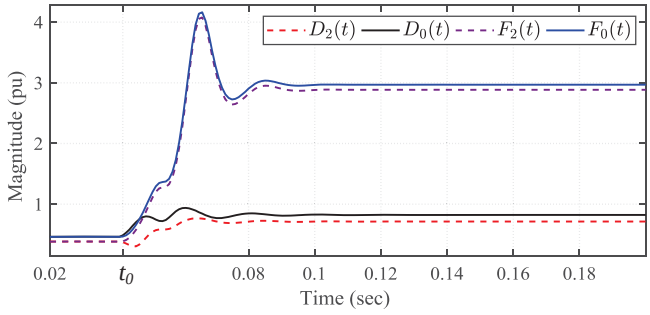

Fig. 11. Estimated $F_i(t)$ $D_i(t)$ before and after single-pole ORCB.

simulations carried out show that the inclusion of even up to 5% total vector error (TVE) [26], in the input phasors does not have a considerable adverse impact on the ORCB indices. As explained earlier, $F_i(t)$ and $D_i(t)$ take the same value before single-pole ORCB, while they become different, afterwards. This can be easily observed from Fig. 11.

To further demonstrate the applicability of the proposed method, the previous simulations are repeated for line lengths of 50, 150, and 200 km. Table I summarizes obtained results. It can be seen that the proposed distance relay remains effective, irrespective of the protected line length. The fault clearing time by the proposed relay is always smaller than that of the conventional one. The time between three- and single-pole ORCB and issuing the local trip command is obtained to be, on average, 32 and 27 ms, respectively.

TABLE I
RELAYING PERFORMANCE ON THE TWO-SOURCE TEST SYSTEM

Line Length		50 km	100 km	150 km	200 km
Distance Relay		Average Fault Clearing Time (ms)			
3-pole	Prop.	100	101	99	102
	Conv.	173	172	172	170
1-pole	Prop.	98	96	97	96
	Conv.	155	157	153	155

TABLE II
RELAYING PERFORMANCE ON THE 39-BUS TEST SYSTEM

Distance Relaying	Conventional		Proposed	
ORCB Mode	3-pole	1-pole	3-pole	1-pole
SIT Coverage (%)	47	46	47	46
AST Coverage (%)	6	13	49	50
Fault Clearing Time (ms)	199	177	93	92

B. General Evaluation of the Proposed Method

The 39-bus test system consists of 34 transmission lines, 12 transformers and 10 synchronous generators. To make simulations as realistic as possible, synchronous generators are modeled with automatic voltage regulator (AVR) and turbine governor controls. The phasor estimation error due to a 200-mHz frequency deviation in the waveform is 0.2% of the waveforms amplitude, which is practically negligible. This amount of frequency deviation is an overstating upper bound and in none of extensive simulations conducted, frequency has decayed so much in less than 100 ms, *i.e.*, the time period of concern to our relay. For power systems with highly reduced inertia where frequency deviations might result in unacceptable phasor estimation errors, the effective phasor estimation approaches presented in [27]–[29] can be used to provide accurate phasors to the relay.

A number of 1-ph-g faults with fault resistances of 0 Ω to 25 Ω are applied at 50 different locations on each transmission line. More than 20000 simulation cases are studied and the obtained results are summarized in Table II. The conventional and proposed distance relays yield identical SIT coverage over the faulted line. AST occurs on around 50% of the line length using the proposed method, which reduces the average fault clearing time to 93 ms and leaves faults on only around 4% of the line length to be cleared in Zone 2 operating time. The conventional relays also provide AST on a small portion of the line length, as the impedance seen by them slightly displaces subsequent to ORCB. It is also observed that the proposed distance relay never operates for faults on neighboring lines, unless in Zone 2 operating time and as backup protection.

For the proposed relay to be able to accelerate the opening of the LCB, the opening of the RCB is a prerequisite. Thus, if the RCB fails to open for a fault on the line end-section, the opening of the LCB cannot be accelerated by the relay and it will open in Zone-2 operating time. This is the case also if the RCB opens, but the local relay fails to detect ORCB.

This article has been accepted for publication in a future issue of this journal, but has not been fully edited. Content may change prior to final publication. Citation information: DOI 10.1109/TPWRD.2019.2957302, IEEE Transactions on Power Delivery

This may be caused, for instance, by large receiving-end SIRs, which make it more difficult for the local relay to detect three-pole ORCB. In both cases, the performance of the proposed relay will be identical to that of the conventional distance relay and the LCB will open in Zone-2 operating time.

C. Real Fault Incident

In this part, the proposed distance relay is tested using a real 1-ph-g fault record from a 160 km 230 kV transmission line. The related CBs are only able to open three-pole. Two distance relays are used in a permissive underreaching transfer trip scheme (PUTT) to provide fast fault clearance over the protected line [4], and the power line carrier (PLC) is deployed as the communication medium.

On one occasion in 2017, a 1-ph-g fault occurred on that line 145 km away from one end of the line, that is α=90.6%. From the fault recorder data of the distance relay at that end of the line, the voltage and current waveforms of the incident have been extracted. Reportedly, one end of the line was opened in Zone 1 operating time, while the other end was opened in Zone 2 operating time. The transfer trip signal was seemingly sent out by the relay close to the fault, but there was no evidence of the reception of that signal by the opposite-end relay.

Fig. 12 shows the three-phase current waveforms recorded by the relay. The fault occurs at t=0 ms, and the three-pole ORCB starts at around t=76 ms and is completed at t_o=130 ms. Subsequent to the three-pole opening of the RCB, the apparent impedance seen by the conventional relay slightly displaces but still remains inside the Zone 2 operating characteristic of the relay. Finally, the line gets disconnected by the LCB after around 470 ms since the fault inception. However, as can be seen from Fig. 9, the proposed relay would disconnect the LCB at t_r=152 ms, once the three-pole ORCB index drops to zero for T_D=10 ms.

V. Conclusions

In this paper, a novel non-communication distance relaying method has been proposed for high-speed protection of the entire length of transmission lines. To achieve this, a protection logic is developed accelerating the relay decision time for faults on the end-sections of the protected line. For such faults, conventional relays disconnect the line in Zone-1 operating time from one side, and in Zone-2 operating time from the opposite side of the line. This is the case regardless of single- or three-pole opening of the remote-end circuit breaker (ORCB). This whole fault-clearing process for end-section faults can be accelerated by a factor of four using the proposed relay. Both proposed and conventional distance relays will operate in Zone-1 operating time for faults lying inside their Zone-1 characteristics.The proposed relay accomplishes Accelerated Sequential Tripping (AST) within a couple of cycles after the ORCB instant.

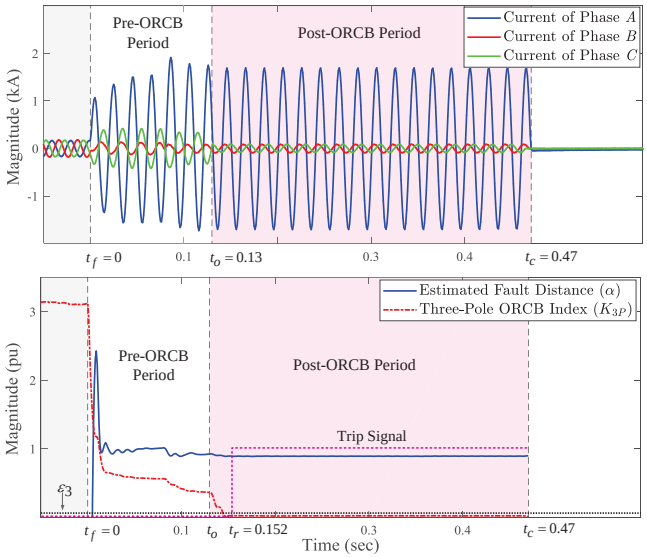

Fig. 12. Three-phase current waveforms, three-pole ORCB index and estimated fault distance for a real fault case.

As detailed in the paper, the fault distance can be accurately obtained based upon the local measurements taken after single- or three-pole ORCB. Providing a high level of security, two sets of indices are developed to infer the instant of three- or single-pole ORCB. As the proposed relay has a modular design, the ORCB indices can be replaced or used in parallel with any other effective indices developed to this end. Contrary to existing AST methods, the proposed relay does not place any constraints on system parameters or operating condition in order to function properly. Fast fault clearing would be provided in this way for nearly 98% of the line length with no need for signaling. AST on the end-sections of the line halves the fault clearing time for 1-ph-g faults. The proposed distance relay can be used individually or in parallel with pilot relaying schemes, to facilitate high-speed protection of the protected line. The method can be easily extended to cover other fault types, as well.

Appendix A
Derivation of (22)

To demonstrate the validity of (22), recall that $\alpha(t)$ and $R_f(t)$ are calculated from

$$\alpha\left(t\right)U_{s,A}\left(t\right)+R_f\left(t\right)I_{s,A}\left(t\right)=V_{s,A}\left(t\right) \tag{A.1}$$

The solution of this equation over time can be denoted as below

$$[\alpha(t),R_f(t)]=\begin{cases}[\alpha,R_f] & \forall\ t_o\le t\\ [\alpha^*,R_f^*] & \forall\ t_f\le\ t\le t_o\end{cases} \tag{A.2}$$

where the asterisk refers to the incorrect values estimated for the corresponding unknowns before ORCB.

Here, in the first step, we justify the following equality:

$$F_i(t)=\begin{cases}I_{r,i}^{fault} & \forall\ t_o\le t\\ \gamma_i I_f^{fault} & \forall\ t_f\le\ t\le t_o\end{cases} \tag{A.3}$$

This article has been accepted for publication in a future issue of this journal, but has not been fully edited. Content may change prior to final publication. Citation information: DOI 10.1109/TPWRD.2019.2957302, IEEE Transactions on Power Delivery

where $F_i(t)$ has been defined such that

$$\alpha(t)U_{s,A}^{fault} + 3R_f(t)\left[I_{s,i}^{fault} + F_i\left(t\right)\right] = V_{s,A}^{fault} \quad \text{(A.4)}$$

From the connection of the sequence circuits for a 1-ph-g fault before ORCB, we have

$$\alpha U_{s,A}^{fault} + 3R_f\left[I_{s,i}^{fault} + I_{r,i}^{fault}\right] = V_{s,A}^{fault} \quad \text{(A.5)}$$

On the other hand, for $t_o \leq t$, $\alpha(t)$ and $R_f(t)$ in (A.4) can be replaced with α and R_f, respectively. Comparing the so-updated (A.4) for $t_o \leq t$, with (A.5) verifies that $F_i(t) = I_{r,i}^{fault}$, and hence, the first equality in (A.3).

With respect to (A.2), (A.4) can be expanded for $t_f \leq t < t_o$ as below

$$\begin{cases} \alpha^* U_{s,A}^{fault} + 3R_f^*[I_{s,0}^{fault} + F_0\left(t\right)] = V_{s,A}^{fault} \\ \alpha^* U_{s,A}^{fault} + 3R_f^*[I_{s,1}^{fault} + F_1\left(t\right)] = V_{s,A}^{fault} \\ \alpha^* U_{s,A}^{fault} + 3R_f^*[I_{s,2}^{fault} + F_2\left(t\right)] = V_{s,A}^{fault} \end{cases} \quad \text{(A.6)}$$

One can easily deduce from (A.6) that

$$I_{s,0}^{fault} + F_0\left(t\right) = I_{s,1}^{fault} + F_1\left(t\right) = I_{s,2}^{fault} + F_2\left(t\right) = X \quad \text{(A.7)}$$

where X is an auxiliary variable denoting the sum inside each pair of brackets. Adding the equations of (A.6) together and dividing the result by 3 yields

$$\alpha^* U_{s,A}^{fault} + R_f^*\left[I_{s,A}^{fault} + F_0\left(t\right) + F_1\left(t\right) + F_2\left(t\right)\right] = V_{s,A}^{fault} \quad \text{(A.8)}$$

Comparing (A.8) with (A.1) written for $t_f \leq t < t_o$, one can conclude that

$$F_0\left(t\right) + F_1\left(t\right) + F_2\left(t\right) = 0 \quad \text{(A.9)}$$

It follows from (A.6)-(A.8) and (16) that

$$X = \frac{1}{3} I_{s,A}^{fault} = \frac{1}{3}\sum_{j=0}^{2} \beta_j I_f^{fault} \quad \text{(A.10)}$$

Having obtained X, $F_i(t)$ can be calculated for $t_f \leq t < t_o$ from (A.7) and (16) as below

$$F_i\left(t\right) = \frac{1}{3}\sum_{j=0}^{2} \beta_j I_f^{fault} - I_{s,i}^{fault} = \gamma_i I_f^{fault} \quad \text{(A.11)}$$

This ends the verification of (A.3).

The derivation of (A.12) below is relatively easy:

$$D_i(t) = \frac{1}{3}\sum_{j=0}^{2} I_{s,j}(t) - I_{s,i}(t) = \begin{cases} I_{r,i}^{post} & \forall\ t_o \leq t \\ \gamma_i I_f^{fault} & \forall\ t_f \leq t \leq t_o \end{cases} \quad \text{(A.12)}$$

The first equality of (A.12), *i.e.*, $D_i(t)$ after ORCB, simply replicates (19). The second equality of (A.12) is obtained by replacing $I_{s,i}(t)$ with its equivalent expression from (16).

Eventually, (A.12) together with (A.3) results in (22).

ACKNOWLEDGEMENT

The first author would like to sincerely thank Dr Sayyed Mohammad Hashemi of University of Toronto for his great help with the validation of the proposed method.

REFERENCES

[1] S. H. Horowitz and A. G. Phadke, *Power System Relaying*, 3rd ed. John Wiley & Sons, 2008.

[2] P. M. Anderson, *Power System Protection*, 1st ed. Wiley-IEEE Press, 1998.

[3] W. A. Elmore, *Protective Relaying: Theory and Applications*. CRC Press, 2003.

[4] ALSTOM, *Network Protection and Automation Guide*, 2002.

[5] S. Azizi, M. Sanaye-Pasand, and M. Paolone, "A modified formula for distance relaying of tapped transmission lines with grounded neutrals," *IEEE Trans. on Power Delivery*, vol. 34, no. 2, pp. 690–699, Apr. 2019.

[6] T. H. Shi, H. Zhang, P. Liu, D. J. Zhang, and Q. H. Wu, "Accelerated trip of power transmission line based on biorthogonal wavelet analysis," in *2000 Power Engineering Society Summer Meeting (Cat. No.00CH37134)*, vol. 3, 2000, pp. 1333–1337 vol. 3.

[7] A. Sharafi, M. Sanaye-Pasand, and P. Jafarian, "Non-communication protection of parallel transmission lines using breakers open-switching travelling waves," *IET Generation, Transmission Distribution*, vol. 6, no. 1, pp. 88–98, Jan. 2012.

[8] A. T. Johns, R. K. Aggarwal, and Z. Q. Bo, "Non-unit protection technique for ehv transmission systems based on fault-generated noise. part 1: signal measurement," *IEE Proceedings - Generation, Transmission and Distribution*, vol. 141, no. 2, pp. 133–140, Mar. 1994.

[9] A. Mahari and M. Sanaye-Pasand, "An accelerated single-pole trip scheme for zone-2 faults of distance relays," *IEEE Trans. on Power Delivery*, vol. 32, no. 2, pp. 678–687, Apr. 2017.

[10] A. G. Phadke and S. H. Horowitz, "Adaptive relaying," *IEEE Computer Applications in Power*, vol. 3, no. 3, pp. 47–51, Jul. 1990.

[11] G. Rosas-Ortiz and T. S. Sidhu, "High-speed backup scheme for zone 2 of non-pilot distance relays," *IET Generation, Transmission Distribution*, vol. 1, no. 6, pp. 938–947, Nov. 2007.

[12] L. Pei, C. Deshu, P. Hua, O. P. Malik, and G. S. Hope, "Analysis of an accelerated trip scheme for faults in the second zone of protection of a transmission line," *IEEE Trans. on Power Delivery*, vol. 5, no. 1, pp. 72–78, Jan. 1990.

[13] C. Deshu, L. Pei, P. Hua, G. S. Hope, and O. P. Malik, "Scheme for accelerated trip for faults in the second zone of protection of a transmission line," *IEEE Trans. on Power Delivery*, vol. 4, no. 2, pp. 942–948, Apr. 1989.

[14] T. S. Sidhu, P. Ye, and M. S. Sachdev, "Accelerated trip scheme for second-zone distance protection," *IEE Proceedings - Generation, Transmission and Distribution*, vol. 150, no. 3, pp. 325–333, May 2003.

[15] H. A. Darwish, T. A. Kawady, A. M. I. Taalab, and O. P. Malik, "Robust non-communication line protection scheme using novel quantities," in *2006 IEEE Power Engineering Society General Meeting*, 2006.

[16] Z. Q. Bo, "Adaptive non-communication protection for power lines bo scheme 1-the delayed operation approach," *IEEE Trans. on Power Delivery*, vol. 17, no. 1, pp. 85–91, Jan 2002.

[17] Z. Q. Bo, "Adaptive non-communication protection for power lines bo scheme. ii. the instant operation approach," *IEEE Trans. on Power Delivery*, vol. 17, no. 1, pp. 92–96, Jan. 2002.

[18] V. Leitloff and P. Bastard, "Novel algorithm for accelerated second zone tripping of non-unit distance protection," in *2001 Seventh International Conference on Developments in Power System Protection (IEE)*, 2001, pp. 434–437.

[19] P. J. Moore and H. Al-Nasseri, "Improved zone 2 acceleration scheme using sound phase seen impedance," in *2004 Eighth IEE International Conference on Developments in Power System Protection*, vol. 2, Apr. 2004, pp. 457–460 Vol.2.

[20] S. Vejdan, M. Sanaye-Pasand, and T. S. Sidhu, "Accelerated zone ii operation of distance relay using impedance change directions," *IEEE Trans. on Power Delivery*, vol. 32, no. 6, pp. 2462–2471, Dec. 2017.
[21] C. A. Desoer and E. S. Kuh, *Basic Circuit Theory*. Tata McGraw-Hill, 2009.
[22] S. Azizi, M. Sun, V. Terzija, and M. Popov, "Noncomunication accelerated sequential tripping for remote-end faults on transmission lines," in *2019 IEEE Milan PowerTech*, Jun. 2019, pp. 1–6.
[23] Matpower: A matlab power system simulation package. [Online]. Available: http://www.pserc.cornell.edu/matpower/
[24] G. Benmouyal, "Removal of dc-offset in current waveforms using digital mimic filtering," *IEEE Trans. on Power Delivery*, vol. 10, no. 2, pp. 621–630, Apr. 1995.
[25] M. Kizilcay and T. Pniok, "Digital simulation of fault arcs in power systems," *International Trans. on Electrical Energy Systems*, vol. 1, no. 1, pp. 55–60, Jan. 1991.
[26] *IEEE Standard for Synchrophasor Measurements for Power Systems*, IEEE Std. C37.118.1-2011, 2011.
[27] A. G. Phadke and J. S. Thorp, *Synchronized Phasor Measurements and Their Applications*, 3rd ed. Springer, 2008.
[28] V. Terzija, V. Stanojevic, M. Popov, and L. van der Sluis, "Digital metering of power components according to ieee standard 1459-2000 using the newton-type algorithm," *IEEE Trans. on Instrumentation and Measurement*, vol. 56, no. 6, pp. 2717–2724, Dec 2007.
[29] V. Terzija and V. Stanojevic, "Two-stage improved recursive newton type algorithm for power quality indices estimation," in *2007 IEEE Power Engineering Society General Meeting*, June 2007.

Sadegh Azizi (M'16–SM'19) received the B.Sc., M.Sc., and Ph.D. degrees all in Electrical Power Engineering from K. N. Toosi University of Technology, Sharif University of Technology, and University of Tehran, Tehran, Iran, in 2007, 2010, and 2016, respectively.

He is currently a Lecturer in Smart Energy Systems in the School of Electronic and Electrical Engineering, University of Leeds. From June 2016 to January 2019, he was with The University of Manchester as a Postdoctoral Researcher leading their work on the protection Work Package of the EU H2020 MIGRATE project, in collaboration with more than twenty European Transmission System Operators (TSOs) and research institutes. He was with the Energy and System Study Center, Monenco Iran Consulting Engineers Co., from 2009 to 2011 and the Iran Grid Management Co., Tehran, Iran, from 2013 to 2016. Since 2014, he has been collaborating with the Distributed Electrical Systems Laboratory at the Swiss Federal Institute of Technology of Lausanne. Dr. Azizi is an Associate Editor of the *International Journal of Electrical Power and Energy Systems*. He is also a task leader of Cigré WG B5.57 which is investigating new challenges of frequency protection in modern power systems. His research interests include applications of wide-area monitoring, protection and control systems, digital protective relays, and applications of power electronics in power systems.

Mingyu Sun (S'15) received the B.Eng. degree in Electrical Engineering from Shandong University, Jinan, China in 2013 and the M.Sc. degree in Electrical Power System Engineering from The University of Manchester, Manchester, UK, in 2014. He is currently working towards the Ph.D. degree in Electrical Engineering at The University of Manchester, Manchester, UK. He has also been an Associate Innovation Engineer with National Grid Electricity Transmission, UK, since 2019. His research interests include application of power electronics in power systems, and wide-area monitoring, protection and control systems.

Gaoyuan Liu (S'19) received the B.Eng.(Hons.) degree with top rank in Electrical and Electronic Engineering from The University of Manchester, Manchester, UK, and B.Eng. degree in Electrical Engineering and its Automation from North China Electric Power University, Beijing, China in 2015. He is currently working towards the Ph.D. degree at The University of Manchester. In November 2019, he was with the Institute of Communication and Power Networks, the University of Leeds, Leeds, UK as a visiting researcher. From March 2017 to January 2019 he has worked on the protection Work Package of the EU H2020 MIGRATE project and since January 2019 he has taken on the leadership of the research team at the University of Manchester. His research interests include wide-area monitoring and protection, system integrity protection schemes and large-scale integration of renewable energy sources.

Marjan Popov (M'95–SM'03) obtained the Dipl-Ing. in Electrical Power Engineering from the University of Saints Cyril and Methodius, Skopje, the Republic of Macedonia in 1993 and the Ph.D. degree in Electrical Power Engineering from Delft University of Technology, Delft, Netherlands, in 2002. He is also a Chevening alumnus and in 1997, he was an Academic Visitor with the University of Liverpool, Liverpool, UK, working in the Arc Research Group on modeling SF6 circuit breakers.

His major fields of interest are in future power systems, large-scale power system transients, intelligent protection for future power systems, and wide-area monitoring and protection. Prof. Popov is a member of Cigré and actively participated in WG C4.502 and WG A2/C4.39. In 2010 he received the prestigious Dutch Hidde Nijland Prize for extraordinary research achievements. He is an IEEE PES Prize Paper Award and IEEE Switchgear Committee Award recipient for 2011 and an Associate Editor of Elsevier's *International Journal of Electrical Power and Energy Systems*.

Vladimir Terzija (M'95-SM'00–F'16) was born in Donji Baraci (former Yugoslavia). He received the Dipl-Ing., M.Sc., and Ph.D. degrees in electrical engineering from the University of Belgrade, Belgrade, Serbia, in 1988, 1993, and 1997, respectively.

He is the Engineering and Physical Science Research Council (EPSRC) Chair Professor in Power System Engineering with the Department of Electrical and Electronic Engineering, The University of Manchester, Manchester, UK, where he has been since 2006. From 1997 to 1999, he was an Assistant Professor at the University of Belgrade, Belgrade, Serbia. From 2000 to 2006, he was a senior specialist for switchgear and distribution automation with ABB, Ratingen, Germany. His current research interests include smart grid applications; wide-area monitoring, protection and control, multi-energy systems, switchgear and transient processes, ICT, data analytics and digital signal processing applications in power systems.

Prof. Terzija is the Editor in Chief of the *International Journal of Electrical Power and Energy Systems*, Alexander von Humboldt Fellow, as well as a DAAD and Taishan Scholar. He is the recipient of the Qilu Friendship Award, China (2018). Since 2018, he is the National Thousand Talents Distinguished Professor at Shandong University, China.